Acta Crystallographica Section D
Biological Crystallography
ISSN 0907-4449

Structure of viscotoxin A3: disulfide location from weak SAD data

Judit É. Debreczeni,[a] Beatrix Girmann,[b] Axel Zeeck,[b] Ralph Krätzner[a] and George M. Sheldrick[a]*

[a]Lehrstuhl für Strukturchemie, Georg-August Universität, Tammannstrasse 4, Göttingen, Germany, and [b]Institut für Organische Chemie, Abteilung Biomolekulare Chemie, Georg-August Universität, Tammannstrasse 2, Göttingen, Germany

Correspondence e-mail: gsheldr@shelx.uni-ac.gwdg.de

Received 7 August 2003
Accepted 27 August 2003

PDB Reference: viscotoxin A3, 1okh, r1okhsf.

The crystal structure of viscotoxin A3 (VT A3) extracted from European mistletoe (*Viscum album* L.) has been solved using the anomalous diffraction of the native S atoms measured in-house with Cu $K\alpha$ radiation to a resolution of 2.2 Å and truncated to 2.5 Å. A 1.75 Å resolution synchrotron data set was used for phase expansion and refinement. An innovation in the dual-space substructure-solution program *SHELXD* enabled the individual S atoms of the disulfide bonds to be located using the Cu $K\alpha$ data; this resulted in a marked improvement in the phasing compared with the use of super-S atoms. The VT A3 monomer consists of 46 amino acids with three disulfide bridges and has an overall fold resembling the canonical architecture of the α- and β-thionins, a capital letter L. The asymmetric unit consists of two monomers related by a local twofold axis and held together by hydrophobic interactions between the monomer units. One phosphate anion (confirmed by ^{31}P-NMR and MS) is associated with each monomer.

1. Introduction

Viscotoxins belong to the pharmacologically important constituents of European mistletoe (*Viscum album* L.) and were first isolated and characterized more than 50 years ago (Winterfeld & Bjil, 1948). Based on their sequence homology, S—S bridge arrangement (Samuelsson *et al.*, 1968; Samuelsson & Pettersson, 1971; Schrader & Apel, 1991; Orrú *et al.*, 1997) and biological role (Florack & Stiekema, 1994), viscotoxins were classified in later studies in the α- and β-thionin family of basic, cysteine-rich and toxic microproteins which can be found in the seeds and leaves of different cereals. To date, at least six different isoforms of viscotoxin have been described (A1, A2, A3, B, 1-PS and U-PS) and a host-dependent variation in the isoform pattern has also been reported (Schaller *et al.*, 2000).

The thionins have been shown to possess a broad spectrum of biological activity, being toxic to either Gram-positive or Gram-negative bacteria, fungi, yeast and various mammalian cell types (Caleya *et al.*, 1972; Evans *et al.*, 1989; Epple *et al.*, 1997). The cytotoxicity of viscotoxins and mistletoe extracts has been investigated in detail on various tumour-cell lines, such as human myeloid cell line K562, human T-cell leukaemia cell line Molt4, Yoshida sarcoma cell and on human granulocytes and lymphocytes (Jung *et al.*, 1990; Urech *et al.*, 1995). In addition to their cytotoxicity, viscotoxins exhibit immunomodulating effects at non-toxic concentrations (Stein, Schaller, Pfüller, Schietzel *et al.*, 1999; Stein, Schaller, Pfüller, Wagner *et al.*, 1999; Tabiasco *et al.*, 2002). In spite of extensive studies on the biological activity of these microproteins, their

mechanism of action has not been definitively clarified. In the early 1980s, viscotoxins were proved to protect DNA against thermal denaturation through ionic binding (Woynarowski & Konopa, 1980). Subsequent experiments showed that thionins are able to permeabilize the cell membrane of various cell types (Carrasco *et al.*, 1981). Two different hypotheses accounting for the lytic effects of thionins, ion-channel formation (Hughes *et al.*, 2000) and membrane disruption through electrostatic interactions (Coulon *et al.*, 2002), were proposed as possible explanations. Structural studies together with electrostatic calculations also suggested interactions with negatively charged molecular targets driven by electrostatic forces (Romagnoli *et al.*, 2000). The present work reports the crystal structure of viscotoxin A3 (VT A3), shedding light on possible anion-binding sites, structural flexibility and molecular association.

Despite recent advances, the phase problem can still pose a barrier to structure solution even when properly diffracting crystals are available. The selenomethionine MAD (multiple-wavelength anomalous diffraction) technique comes nearest to providing a general experimental solution, especially for recombinant proteins, but can be problematic to apply to substances isolated from natural sources. Molecular replacement may be hampered by an inadequate model and is less effective when the solvent content is low. The preparation of heavy-atom derivatives by soaking can also fail when the structure is tightly packed and presents no suitable binding sites. Since VT A3 was isolated from a natural source, contains no methionine and all our attempts at molecular replacement and classical heavy-atom derivatization failed, we decided to carry out a sulfur-SAD (single-wavelength anomalous diffraction) experiment to take advantage of the weak anomalous scattering of the S atoms in the three disulfide units per molecule.

After an encouraging start over 20 years ago (Hendrickson & Teeter, 1981) and the development of computational methods for improving the raw SAD phases (Wang, 1985), there was little progress in sulfur-SAD phasing until recent improvements in detector hardware and processing software, high-intensity sources and the widespread use of cryo-crystallography enabled the small anomalous intensity differences (*ca* 1.5%) to be measured with the necessary precision. Recent examples have shown that the S atoms inherently present in proteins can indeed be employed to phase proteins even at the Cu $K\alpha$ wavelength, provided the anomalous signal can be measured precisely enough (Dauter *et al.*, 1999; Liu *et al.*, 2000; Yang & Pflugrath, 2001; Lemke *et al.*, 2002; Debreczeni, Bunkóczi, Girmann *et al.*, 2003; Debreczeni, Bunkóczi, Ma *et al.*, 2003), although longer wavelengths have also been employed to enhance the anomalous signal from sulfur (Gordon *et al.*, 2001; Weiss *et al.*, 2001; Brown *et al.*, 2002; Micossi *et al.*, 2002). High redundancy and a wide distribution of equivalent reflections over different data frames are necessary for good scaling and merging and hence the measurement of precise data; this is best achieved with a three-circle or κ goniometer, although high symmetry also helps. The production of high-quality maps from SAD data is facilitated by high-resolution native data, a high solvent content and non-crystallographic symmetry. In this particular case, the rather low solvent content counterbalanced the beneficial effects of the twofold non-crystallographic symmetry and an innovation enabling the location of the individual atoms of the S—S super-sulfur moieties was required for success.

2. Experimental

2.1. Purification

Dried powdered plant material collected from poplar trees was extracted with 2% acetic acid and the resulting extract was concentrated and passed through a cation-exchange column (SP Sephadex C-25, eluted with 1 *M* ammonium acetate). The raw product was further purified using MPLC (LiChroprep RP-8, eluted with 40% acetonitrile, 0.1% TFA). Viscotoxin isoforms were separated by HPLC (Nucleosil 100 C8 and Phenomenex C18 5 µm, eluted with a water–acetonitrile gradient in the presence of 0.1% TFA). It should be noted that no phosphate-containing chemicals were used during isolation and purification.

2.2. Crystallization

Crystallization was carried out using the hanging-drop technique at room temperature with droplets containing equal volumes of the protein solution (15 mg ml^{-1} VT A3 in water) and reservoir solution [0.15 *M* $(NH_4)_2SO_4$, 0.05 *M* cacodylate buffer pH 6.5, 30% PEG 8000, 15 m*M* $HgCl_2$]. Needle-shaped crystals of approximate dimensions 0.1 × 0.1 × 1.0 mm were obtained in 1–2 weeks.

2.3. Data collection

A VT A3 crystal was mounted with a loop in an arbitrary orientation and flash-cooled in a nitrogen stream to 100 K. 25% glycerol was used for cryoprotection. A highly redundant 2.2 Å data set was then collected on a Bruker rotating-anode generator equipped with Osmic focusing mirrors, a three-circle goniometer and a Bruker Smart6000 4K CCD detector. The data set was processed using the Bruker programs *PROTEUM*, *SAINT* and *SADABS*, and analysed with *XPREP* (Bruker Nonius, 2002).

For phase-extension and refinement purposes, a 1.75 Å synchrotron data set was also collected at the X31 beamline at EMBL/DESY. In this case, *DENZO* and *SCALEPACK* (Otwinowski & Minor, 1997) were used for data processing. Data-collection statistics are listed in Table 1. The merging *R* value (based on intensities) between the in-house and synchrotron data was 11.4%.

2.4. Phase determination, model building and refinement

The heavy-atom substructure was solved using *SHELXD* (Sheldrick *et al.*, 2001). Solutions were identified by high values of the correlation coefficient. Without any further refinement, the heavy-atom parameters were fed into

Table 1
Data-collection statistics.

Values in parentheses refer to the last resolution shell.

	In-house	Synchrotron
Space group	$P2_12_12$	$P2_12_12$
Unit-cell parameters (Å)	a = 47.70, b = 68.77, c = 25.35	a = 48.00, b = 68.59, c = 25.26
Data collected	333468	50787
Unique data	4490	8938
Resolution (Å)	2.20 (2.30–2.20)	1.75 (1.85–1.75)
Completeness	96.8 (75.3)	100.0 (99.7)
Redundancy	71.9 (4.9)	5.3 (4.4)
$R_{\rm int}$ (%)	4.9 (10.9)	8.9 (38.7)
Average $I/\sigma(I)$	93.9 (12.6)	14.3 (3.9)

Table 2
Model refinement statistics.

Resolution range	20.0–1.75
No. of protein residues	92
No. of non-H atoms	780
No. of water molecules	94
R factor/$R_{\rm free}$ (%)	16.7/23.9
R.m.s.d. from ideal geometry	
Bond length (Å)	0.006
Angle distances (Å)	0.021
Ramachandran plot (%)	
Allowed region	100
Generously allowed region	0
Disallowed region	0
Mean B values	
Protein	16
Water	33
Anions (all atoms)	36

SHELXE (Sheldrick, 2002) for phasing and density modification. NCS averaging was then performed from the heavy-atom coordinates and an NCS mask generated from the sulfur positions using the *CCP*4 (Collaborative Computational Project, Number 4, 1994) program *NCSMASK*. The initial model was built by *ARP*/*wARP* (Perrakis *et al.*, 1999), visualized with *XtalView* (McRee, 1999) and refined against the 1.75 Å synchrotron data set with *SHELXL* (Sheldrick & Schneider, 1997). The stereochemistry of the final model was assessed with *PROCHECK* (Laskowski *et al.*, 1993). A summary of the refinement statistics is given in Table 2.

3. Heavy-atom substructure solution and phasing

To ensure high data redundancy, four 360° φ scans and nine 180° ω scans were collected with thin slicing (0.2°). Scans were arranged in such a way that data resulting from φ and ω scans were of approximately equal redundancy, resolution and completeness. The correlation coefficient CC between the signed anomalous differences for the two scan modes was used to establish the resolution limit of the anomalous signal, so the φ and ω scans were therefore first treated separately. For the purpose of heavy-atom location, all data were then scaled together in a single *SADABS* run. For the original location of super-S atoms (which tends to work better at lower resolution so that the disulfides behave more like single atoms) the data were truncated at 3.0 Å. It can be seen in Fig. 1 that there is a sharp drop in CC at 2.5 Å resolution where it has the value of 30%, so for the purpose of disulfide-bond resolution with the new algorithm (see below) the data were truncated at this point. The completeness, redundancy and mean $I/\sigma(I)$ were 100%, 41% and 48, respectively, for the 2.5–2.6 Å shell; Debreczeni, Bunkóczi, Ma *et al.* (2003) recommended truncating the data at an $I/\sigma(I)$ of about 30 for substructure solution.

It can been seen from Fig. 1 that the CC is much more sensitive to the quality of the anomalous signal than is the ratio of the anomalous difference dF to its standard deviation. We attribute this to the use of the *signed* anomalous differences in calculating CC, whereas only the *unsigned* values (with less information content) can be used for dF. Moreover, CC goes to zero when the noise swamps the anomalous signal, whereas dF gradually approaches a value in the region of 1.0 that is rather sensitive to the accuracy of the estimation of the standard deviations in the anomalous differences; these standard deviations are notoriously difficult to estimate with high accuracy. We are assuming that the φ and ω scans can be treated as independent experiments, but if a three-circle or κ goniometer is not available it should still be possible to calculate CC from measurements on two separate crystals or to rotate a single crystal using a goniometer head fitted with an arc between the two scans.

The ratio $\sum|I_+ - I_-|/\sum(I_+ + I_-)$ from the calculated

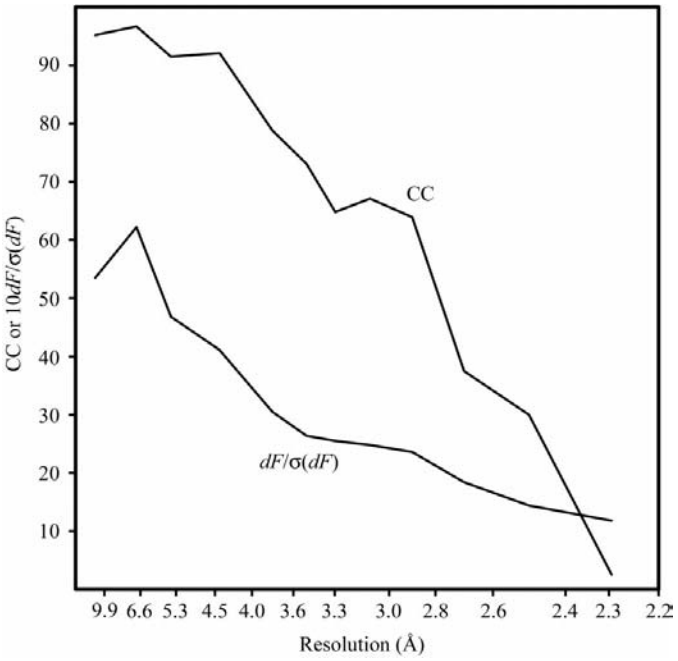

Figure 1
The correlation coefficient CC (%) between the signed anomalous differences of the φ and ω scans and the mean value of the unsigned anomalous difference dF divided by its standard deviation. For the purpose of heavy-atom location with disulfide resolution, the data were truncated at 2.5 Å, where CC drops below 30%. CC appears to be more sensitive to the quality of the anomalous signal with a sharp drop at 2.5 Å and it is not affected by difficulties in estimating precise standard deviations for the anomalous differences.

structure factors using complex scattering factors for the final refined structure is 0.012, which is probably slightly higher than average for a protein; this calculated value is a more realistic indication of the amount of anomalous scattering than an estimate from the scattering factors ignoring disorder and assuming that all atoms have the same B values.

Six super-S atoms were found by *SHELXD* corresponding to six disulfide bridges and indicating the presence of two molecules in the asymmetric unit with an estimated solvent content of 32% (Fig. 2*a*). The correlation coefficients between E_o and E_c output by *SHELXD* were 30.87% (all data) and 11.16% (weak data). The heavy-atom positions also allowed us to derive the NCS operator. However, the map after *SHELXE* phasing and density modification proved not to be interpretable and NCS averaging with the *CCP*4 (Collaborative Computational Project, Number 4, 1994) program *DM* did not improve it at all. After successful structure solution, a post-mortem analysis showed that there was very little initial phase information, apparently not enough to adequately define the initial molecular envelope and NCS masks.

Previous experience gained from measurements on test crystals (Debreczeni, Bunkóczi, Ma *et al.*, 2003) suggested that the precision of the heavy-atom model was insufficient to obtain acceptable phases and that the low solvent content hindered the phase-improvement stage. To improve the heavy-atom model, *SHELXD* was modified to introduce a little chemical information, namely that the super-S atoms are actually disulfides. The modification was implemented in the peak-search routine that is used in each dual-space refinement cycle. First, a normal peak-search is performed (rejecting any peak closer than say 3.5 Å to a higher peak) to find the super-S atoms plus any other anomalous scatterers (in VT A3 there are no methionines, but one suspected sulfate is found in the peak list). The positional coordinates of the super-S atoms sometimes correspond to the middle of the S—S bond, but more often they are closer to one or other of the two S atoms. Each peak in this peak list is then tested to see if it can be better fitted by an S—S unit with an S—S distance of 2.06 Å than by a single atom and the best position and orientation of the S—S unit is found by a local optimization of its fit to the observed density. The S—S unit is preferred to a single atom if the sum of the densities at the two sulfurs is greater than 1.3 times the height of the original (super-sulfur) peak. This algorithm works particularly well in the intermediate resolution region (2.0–2.8 Å) in which the two S atoms may or may not be resolved from one another in the electron density. Since only the regions around the highest peaks are analysed in this way, the extra computer time required is negligible.

In practice, the new algorithm enables the data to be truncated at a somewhat higher resolution than for a super-sulfur search alone. The data for VT A3 were truncated at 2.5 Å, the resolution which the correlation coefficient of 30% between the signed anomalous differences for the φ and ω scans indicated as the limit of significant anomalous signal (Schneider & Sheldrick, 2002). The modified *SHELXD* found all six disulfide bridges, one putative sulfate and one noise peak with appreciably higher correlation coefficients between E_o and E_c (37.8, 16.0%) than for the super-sulfurs alone, indicating an improvement in the heavy-atom substructure (Fig. 2*b*). With these atoms as input without further refinement of their coordinates and the full 1.75 Å synchrotron data as native, *SHELXE* gave a good discrimination between the two heavy-atom enantiomorphs and a map with a map correlation coefficient of 0.71 relative to the final refined structure that was almost certainly traceable by hand (but not by *ARP*/*wARP* using default settings). After NCS averaging, the map correlation coefficient rose to 0.84 and the map allowed autobuilding with *ARP*/*wARP*. Figs. 3 and 4 show the progress of phase improvement.

4. Structure description

4.1. Overall fold

The overall fold of VT A3 resembles the canonical architecture of α- and β-thionins, a capital letter L (Hendrickson & Teeter, 1981). The long arm of this letter is an antiparallel pair of helices, while the short arm is defined by two antiparallel β-strands. Residues 6–18 and 22–30 are involved in the

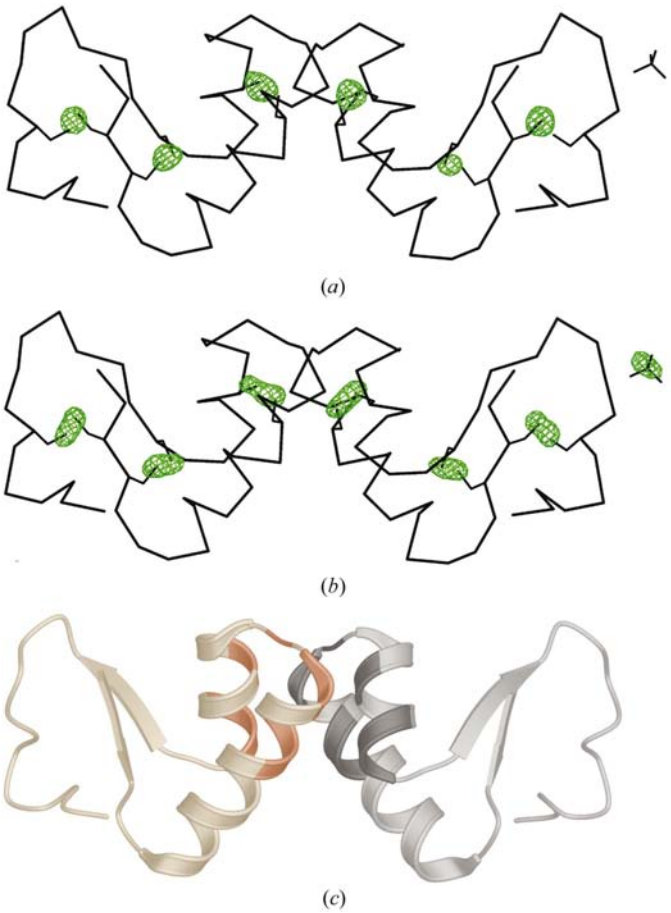

Figure 2
Anomalous Fourier maps contoured at 4.5σ (phases from *SHELXE* after density modification) showing (*a*) six super-S atoms around the disulfide bridges and (*b*) resolved S atoms and a sulfate anion; (*c*) ribbon diagram of the hydrophobic type dimer. Residues constituting the dimer interface are represented in darker colours. The full 2.2 Å in-house anomalous data were used for (*a*) and (*b*).

formation of the helices, stabilized by a number of intrahelical hydrogen bonds and a disulfide bridge between residues 16 and 26. The β-strands are comprised of residues 1–5 and 32–37, linked by four hydrogen bonds and a disulfide bridge between residues 4 and 32. The C-terminal part of the protein chain forms a coil fixed by mainly hydrophobic interactions and a disulfide bridge between residues 3 and 40.

The two arms of the letter L are connected by a hydrogen-bonding and salt-bridge network involving the highly conserved residues 2, 4, 10 and 46. The C-terminal carboxyl group binds the guanidinium group of Arg10 with a salt bridge and the N atom of Cys4 through a hydrogen bond. Both the side-chain and main-chain O atoms of Ser2 form hydrogen bonds to the guanidinium group of Arg10.

This pattern of stabilizing forces is rather conserved among the α- and β-thionins and provides the molecule with a high degree of rigidity. However, flexibility of the molecule can be expected at the hinge region in spite of the stabilizing quartet of residues 2, 4, 10 and 46, since no covalent bonds fix the relative position of the two arms in the letter L.

Two nearly equivalent molecules were found in the asymmetric unit, connected by a non-crystallographic twofold axis forming a hydrophobic type dimer. Least-squares superposition of the molecules gave an r.m.s.d. of 0.41 Å for all main-chain atoms, proving the high conformational similarity.

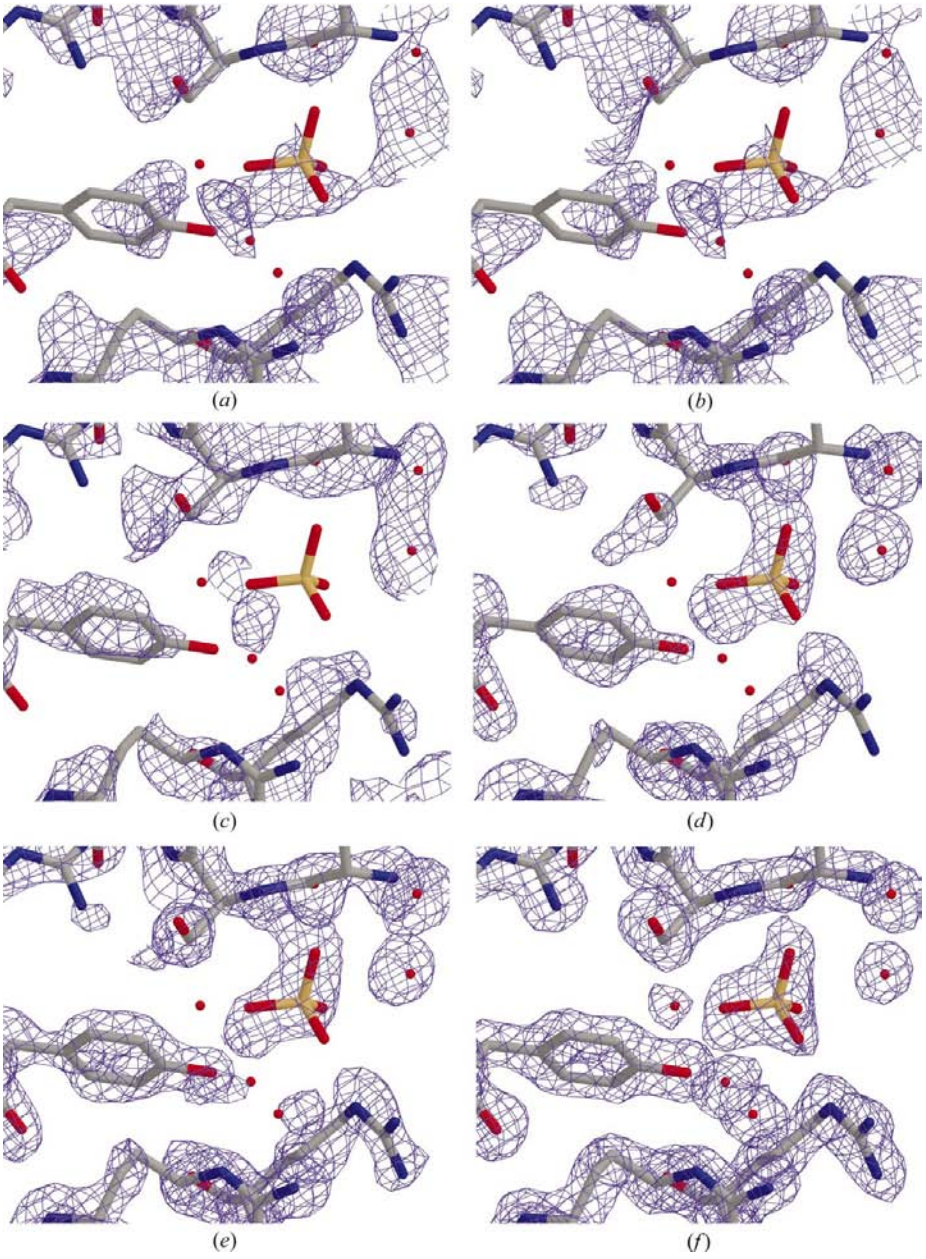

Figure 3
Electron-density maps contoured at 1.0σ around the ordered phosphate ion calculated in different stages of phase improvement: (*a*) initial phases and (*b*) after density modification in *SHELXE*, disulfides not resolved; (*c*) initial phases and (*d*) after density modification in *SHELXE*, disulfides resolved; (*e*) after NCS averaging in *DM*; (*f*) final refinement. The full 1.75 Å native synchrotron data were used with figure of merit or σ_A weights for all these maps.

4.2. Comparison with the NMR models

The crystal structure of VT A3 shows an r.m.s.d. of 1.2–1.4 Å when superimposed on the NMR models (Romagnoli *et al.*, 2000; PDB code 1ed0). As illustrated in Fig. 5, models superimposed between residues 8 and 28 indicate clear differences in the relative positions of the two major domains. The short β-sheets are displaced towards the helices in the crystal structure; therefore, the entire molecule adopts a closed conformation. The C-terminal end and the first few residues connected to it are less precisely determined in the NMR structures, but it is worthy of note that the conformational variance amongst the ten deposited NMR structures is smaller than the structural difference between the X-ray and NMR models. Similar results were obtained when VT A3 was compared with the recently determined hellethionin-D structure (Milbradt *et al.*, 2003; PDB code 1nbl).

4.3. Phosphate-binding sites

A tetrahedral anion bound to the negatively charged groove between the two domains of the L-structure can account for the closed conformational state of both molecules in the asymmetric unit. These anions were refined as phosphates based on the following findings (Girmann, 2003). Mass spectra indicated an additional VT A3 peak with a 98 Da mass difference corresponding to a phosphate adduct.

^{31}P-NMR spectra with a single peak at 2.03 p.p.m. relative to phosphoric acid also showed the presence of non-covalently bound phosphate in the purified sample, although no phosphate-containing chemicals were used during isolation and purification. Photometric phosphate determination indicated phosphate in the sample after hydrolysing the protein.

The ordered sulfate and phosphate anions had *B* values of 28 and 32 Å^2; the second phosphate is disordered over two sites with *B* values of 37 and 42 Å^2. In the anomalous Fourier map based on the phases after density modification with *SHELXE* (with 90° subtracted; Fig. 2*b*) the sulfate corresponded to a 7σ peak and the ordered phosphate to 6σ, whereas the two P sites of the disordered phosphate corresponded to peaks of height 2.5σ. When this map was calculated using the phases from the final refinement as a basis, the peak heights were very similar (6, 6, 3.5 and 3.5σ, respectively).

One of the O atoms of the phosphate ion is hydrogen bonded directly to the N$^{\varepsilon}$ atom of Arg23, while the interaction with the N$^{\varepsilon}$ atom of Arg17 is mediated by a water molecule. Another phosphate oxygen forms hydrogen bonds with the OH groups of Tyr13 and of Ser2. The backbone N atoms of Lys1 and Ser2 are also involved in the anion binding (Fig. 6).

The arrangement of the coordinating side chains is essentially identical between the two monomers. However, the binding pockets of the monomers differ in two features. Ser42 of a symmetry-equivalent molecule forms connections with the O atoms of the phosphate in the first molecule, while this interaction is missing in the second case. As a result, the phosphate anion of the second molecule is disordered and is partially displaced towards the solvent region.

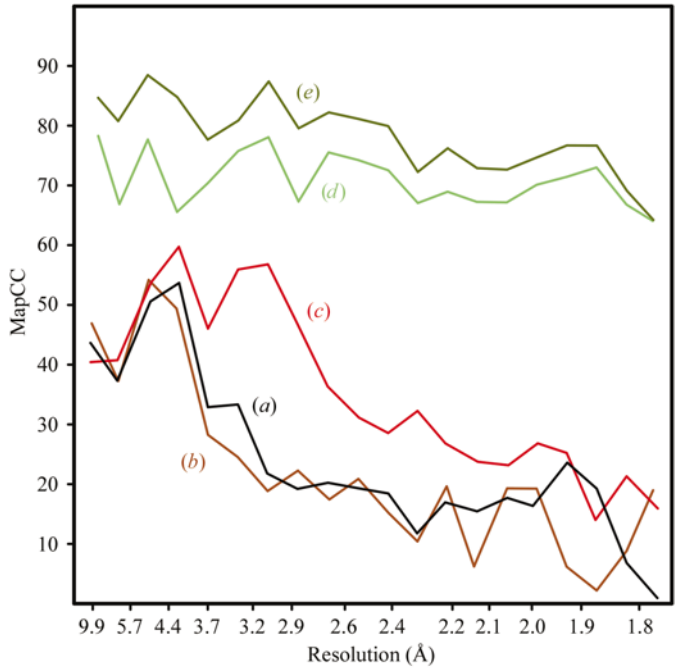

Figure 4
The map correlation coefficient as function of resolution in different stages of phase improvement. The labels correspond to those of Fig. 3.

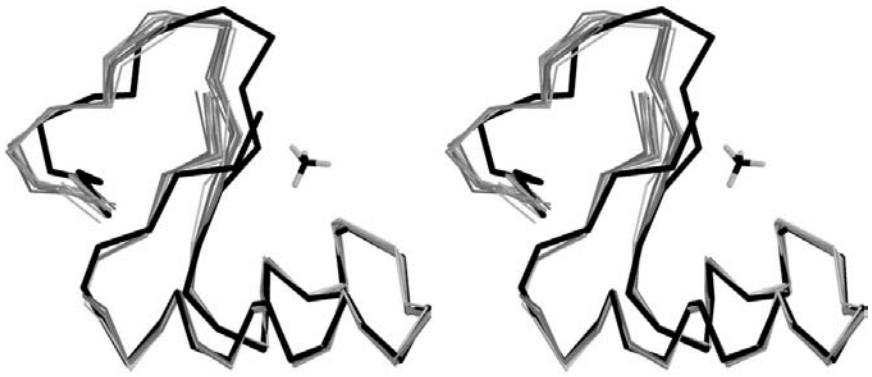

Figure 5
Stereoview of the backbone representation of VT A3: the X-ray structure (black) superimposed on the NMR models (grey).

4.4. Dimerization and crystal packing

As a consequence of the extremely low solvent content, there are several interactions between the molecules in the crystal structure. These mostly involve hydrogen bonds mediated by a number of ordered structural water molecules. There are, however, two intermolecular interactions that can be considered to play a major role in crystal lattice formation. Firstly, as mentioned above, the two molecules in the asymmetric unit build a hydrophobic type dimer. The apolar residues Ala15, Cys16, Ala21 and Leu29 together with the hydrophobic groups of the residues Thr19, Thr25 and Lys28 form the dimer interface between the two monomers (Fig. 2*c*). The hydrophobic surfaces of the amphipathic helices are therefore protected from direct contact with the solvent.

In addition to the hydrophobic type of molecular association, strong hydrophilic contacts can also be found. The strongest of these involves the binding of a sulfate anion and leads to a tight packing of four molecules around the crystallographic twofold axis. As shown in Fig. 6, the sulfate ion is coordinated by three molecules: the first molecule of the asymmetric unit and by two symmetry equivalents of the second one. The backbone N atoms of Thr39 and Ser38 of the first molecule and the guanidinium groups of Arg17 and Arg23 in one of the symmetry mates of the second one form a pocket with relatively high positive electrostatic potential in which the sulfate ion is bound. This pseudo-tetrameric association of the molecules is strengthened by the contact between the sulfate ion and the side-chain O atoms of Thr39 and Ser36.

The crystal packing of VT A3 resembles that of α- and β-purithionin (Rao *et al.*, 1995; Stec *et al.*, 1995) since all of these crystals contain tetrameric associations of molecules that constitute layers. Unlike purothionins, further association of VT A3 tetramers to layers is attained by the hydrophobic dimerization of the VT A3

molecules; the contact between the tetramers in the plane of the layers is thus hydrophobic. In contrast, the interactions between the layers can be characterized as rather weak, as they only involve weak hydrogen bonds mediated by solvent molecules.

5. Biological implications

Previous studies on the cytotoxic effect of thionins and the related viscotoxins have proved that these microproteins are able to disrupt the membrane integrity of many types of cells and have revealed a strong correlation between the cytotoxicity of the different toxins and their capability for membrane permeabilization (Thevissen *et al.*, 1996). Since the α- and β-thionins and viscotoxins possess very similar three-dimensional structures with little conformational variance, the sometimes striking differences in their biological activity should therefore be accounted for by specific positions in their amino-acid sequence.

The primary structure of viscotoxins is highly conserved: three-quarters of the sequence is identical amongst the different isoforms. Most of the variable amino acids can be found in the central region of the protein chain between positions 12 and 30. Interestingly, all conserved residues in this region either have structure-stabilizing functions or are involved in phosphate binding.

Residue Tyr13 was previously identified as a key residue for toxicity. The diiodination or nitration of Tyr13 in purothionins led to complete loss of their activity (Wada *et al.*, 1982; Evans *et al.*, 1989). This finding suggested that this single Tyr residue is essential for membrane binding, which was later supported by X-ray crystallography studies: in the molecular structure of these toxins a glycerol molecule is bound in the pocket around Tyr13 (Rao *et al.*, 1995; Stec *et al.*, 1995). In contrast, the highly conserved Tyr13 of the VT A3 is involved in phosphate binding, suggesting a different mechanism of action.

Electrostatic forces were hypothesized to play a role in the interaction with the charged head groups of membrane components, which was supported by the finding that their charge is strongly correlated with their toxicity. Both VT A3 and β-purothionin display an overall high positive electrostatic potential, especially between the two arms of the letter L. In addition, VT A3 shows a larger difference in the potential between the two faces of the molecule, *i.e.* around the binding pocket and the dimer interface. A polycationic structure alone, such as a poly-Lys, poly-Arg or the unfolded VT A3, would probably not be sufficient to trigger cell lysis (Büssing *et al.*, 1999). It is therefore supposed that the positively charged binding pocket is an indispensable condition for interaction with the negatively charged groups of the membrane, but there may be additional structural factors that can influence molecular interactions with membrane components and determine the toxicity. The residues constituting the binding pocket belong to the most conserved amino acids in the viscotoxin sequences, thus they cannot account for the differences in the toxic activity.

The hydrophobic residues constituting the dimer interface in the VT A3 structure vary considerably among the different isoforms. As described by Büssing *et al.* (1999), variations in the side chain of the residue at position 25 (Thr in VT A3, Val in VT A2 and Arg in VT B), *i.e.* in the non-conserved region, can influence the cytotoxic potential enormously. In VT A3 this position is a Thr residue that takes part in the dimer formation. Its substitution by a larger and positively charged Arg could therefore introduce steric and electrostatic changes in the dimer interface. It is supposed that in addition to the presence of an intact (not iodinated) and positively charged binding pocket, a sterically accessible hydrophobic face is also necessary for membrane interactions. The variability of side chains at the dimer interface may allow the specific binding of different membrane constituents and offer various patterns for molecular recognition. This assumption is further supported by the observed flexibility of the molecule at the hinge region between the two arms of the letter L, which is illustrated by the conformational differences between the NMR and X-ray models (Fig. 5).

The questions as to whether the dimer connected by hydrophobic interactions or the tetramer-like associate correspond to the physiological unit and whether they play any role in membrane disruption remain open. There are, however, indications that thionins associate at higher concentrations (Ohtani *et al.*, 1977; Milbradt *et al.*, 2003). A

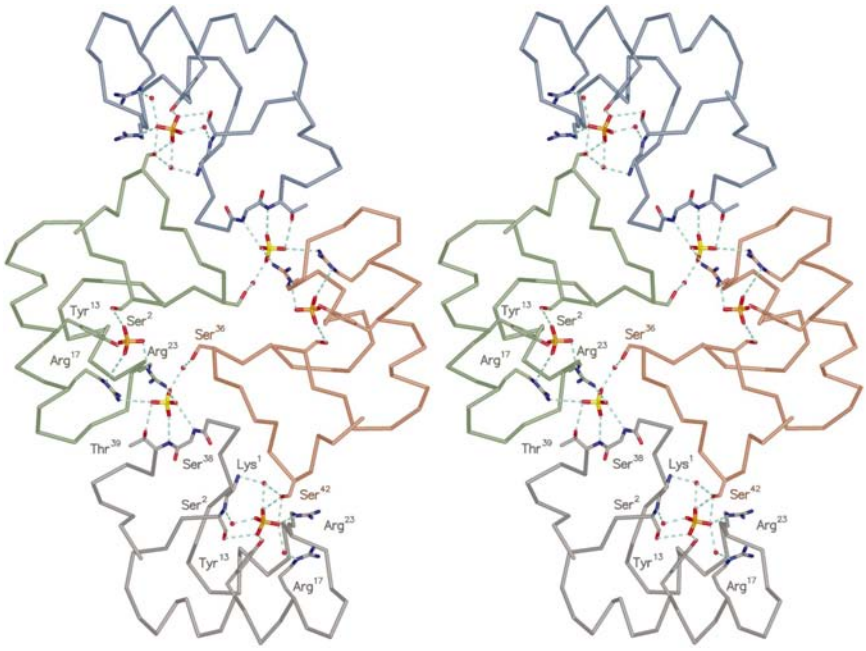

Figure 6
Stereoview of the tetrameric association of VT A3 molecules around the twofold crystallographic axis.

higher stability of the hydrophobic dimer can be assumed in the case of viscotoxins, since most of the hydrophobic residues are protected from the solvent through this association.

We are grateful to Isabel Usón, Thomas R. Schneider and Gábor Bunkóczi for discussions, to Armin Scheffler (Carl Gustav Carus-Institut, Niefern-Öschelbronn) for providing us with purified viscotoxins as comparison samples and to the Fonds der Chemischen Industrie, the DFG (SFB416) and the EU (HPRI-1999-CT-00017 to EMBL/DESY) for support.

References

Brown, J., Esnouf, R. M., Jones, M. A., Linnell, J., Harlos, K., Hassan, A. B. & Jones, E. Y. (2002). *EMBO J.* **21**, 1054–1062.
Bruker Nonius (2002). *PROTEUM*, *SAINT*, *SADABS* and *XPREP* computer programs.
Büssing, A., Stein, G. M., Wagner, M., Wagner, B., Schaller, G., Pfüller, U. & Schietzel, M. (1999). *Eur. J. Biochem.* **262**, 79–87.
Caleya, R. F. D., Gonzalez-Pascual, B., García-Olmedo, F. & Carbonero, P. (1972). *Appl. Microbiol.* **23**, 998–1000.
Carrasco, L., Vázquez, D., Hernández-Lucas, C., Carbonero, P. & García-Olmedo, F. (1981). *Eur. J. Biochem.* **116**, 185–189.
Collaborative Computational Project, Number 4 (1994). *Acta Cryst.* D**50**, 760–763.
Coulon, A., Berkane, E., Sautereau, A.-M., Urech, K., Rougé, P. & Lopez, A. (2002). *Biochim. Biophys. Acta*, **1559**, 145–159.
Cowtan, K. (1994). *Jnt CCP4/ESF–EACBM Newsl. Protein Crystallogr.* **31**, 34–38.
Dauter, Z., Dauter, M., de La Fortelle, E., Bricogne, G. & Sheldrick, G. M. (1999). *J. Mol. Biol.* **289**, 83–92.
Debreczeni, J. É., Bunkóczi, G., Girmann, B. & Sheldrick, G. M. (2003). *Acta Cryst.* D**59**, 393–395.
Debreczeni, J. É., Bunkóczi, G., Ma, Q., Blaser, H. & Sheldrick, G. M. (2003). *Acta Cryst.* D**59**, 688–696.
Epple, P., Apel, K. & Bohlmann, H. (1997). *Plant Cell*, **9**, 509–520.
Evans, J., Wang, Y., Shaw, K.-P. & Vernon, L. P. (1989). *Proc. Natl Acad. Sci.* **86**, 5849–5853.
Florack, D. E. & Stiekema, W. J. (1994). *Plant Mol. Biol.* **26**, 25–37.
Girmann, B. (2003). PhD thesis, University of Göttingen, Germany.
Gordon, E. J., Leonard, G. A., McSweeney, S. & Zagalsky, P. F. (2001). *Acta Cryst.* D**57**, 1230–1237.
Hendrickson, W. A. & Teeter, M. M. (1981). *Nature (London)*, **290**, 107–113.
Hughes, P., Whitecross, M., Llevellyn, D. & Gage, P. (2000). *J. Biol. Chem.* **275**, 823–827.
Jung, M. L., Baudino, S., Ribereau-Gayon, G. & Beck, J. P. (1990). *Cancer Lett.* **51**, 103–108.
Laskowski, R. A., MacArthur, M. W., Moss, D. S. & Thornton, J. M. (1993). *J. Appl. Cryst.* **26**, 283–291.
Lemke, C. T., Smith, G. D. & Howell, P. L. (2002). *Acta Cryst.* D**58**, 2096–2101.
Liu, Z.-J., Vysotski, E. S., Chen. C.-J., Rose, J. P., Lee, J. & Wang, B.-C. (2000). *Protein Sci.* **9**, 2085–2093.
McRee, D. E. (1999). *J. Struct. Biol.* **125**, 156–165.
Micossi, E., Hunter, W. N. & Leonard, G. A. (2002). *Acta Cryst.* D**58**, 21–28.
Milbradt, A. G., Kerek, F., Moroder, L. & Renner, C. (2003). *Biochemistry*, **42**, 2404–2411.
Ohtani, S., Okada, T., Yoshizumi, H. & Kagamiyama, H. (1977). *J. Biochem.* **82**, 753–762.
Orrú, S., Scaloni, A., Giannattasio, M., Urech, K., Pucci, P. & Schaller, G. (1997). *J. Biol. Chem.* **378**, 989–996.
Otwinowski, Z. & Minor, W. (1997). *Methods Enzymol.* **276**, 307–326.
Perrakis, A., Morris, R. J. & Lamzin, V. S. (1999). *Nature Struct. Biol.* **6**, 458–463.
Rao, U., Stec, B. & Teeter, M. M. (1995). *Acta Cryst.* D**51**, 904–913.
Romagnoli, S., Ugolini, R., Fogolari, F., Schaller, G., Urech, K., Giannattasio, M., Ragona, L. & Molinari, H. (2000). *Biochem. J.* **350**, 569–577.
Samuelsson, G. & Pettersson, B. (1971). *Acta Chem. Scand.* **25**, 2048–2054.
Samuelsson, G., Seger, L. & Olson, T. (1968). *Acta Chem. Scand.* **22**, 2624–2642.
Schaller, G., Urech, K. & Grazi, G. (2000). *Mistilteinn*, **2000/1**, 32–40.
Schneider, T. R. & Sheldrick, G. M. (2002). *Acta Cryst.* D**58**, 1772–1779.
Schrader, G. & Apel, K. (1991). *Eur. J. Biochem.* **198**, 549–553.
Sheldrick, G. M. (2002). *Z. Kristallogr.* **217**, 644–650.
Sheldrick, G. M., Hauptman, H. A., Weeks, C. M., Miller, M. & Usón, I. (2001). *International Tables for Crystallography*, Vol. *F*, edited by E. Arnold & M. Rossmann, pp. 333–351. Dordrecht: Kluwer Academic Publishers.
Sheldrick, G. M. & Schneider, T. R. (1997). *Methods Enzymol.* **277**, 319–141.
Stec, B., Rao, U. & Teeter, M. M. (1995). *Acta Cryst.* D**51**, 914–924.
Stein, G. M., Schaller, G., Pfüller, U., Schietzel, M. & Büssing, A. (1999). *Anticancer Res.* **19**, 1034–1042.
Stein, G. M., Schaller, G., Pfüller, U., Wagner, M., Wagner, B., Schietzel, M. & Büssing, A. (1999). *Biochim. Biophys. Acta*, **1426**, 80–90.
Tabiasco, J., Pont, F., Fournié, J.-J. & Vercellone, A. (2002). *Eur J. Biochem.* **269**, 2591–2600.
Thevissen, K., Ghazi, A., De Samblanx, G. W., Osborn, R. W. & Broekaert, W. F. (1996). *J. Biol. Chem.* **271**, 15018–15025.
Urech, K., Schaller, G., Ziska, P. & Giannattasio, M. (1995). *Phytother. Res.* **9**, 49–55.
Wada, K., Ozaki, Y., Matsubara, H. & Yoshizumi, H. (1982). *J. Biochem.* **91**, 257–263.
Wang, B.-C. (1985). *Methods Enzymol.* **115**, 90–112.
Weiss, M. S., Sicker, T. & Hilgenfeld, R. (2001). *Structure*, **9**, 771–777.
Winterfeld, K. & Bjil, L. H. (1948). *Liebig's Ann.* **561**, 107–115.
Woynarowski, J. M. & Konopa, J. (1980). *Z. Physiol. Chem.* **361**, 1535–1545.
Yang, C. & Pflugrath, J. W. (2001). *Acta Cryst.* D**57**, 1480–1490.